Dear Professor Xavier Querol,

Thank you very much for handling our manuscript submitted to ***Atmospheric Chemistry and Physics*** (**MS No.:** egusphere-2023-479; **Title:** Summertime response of ozone and fine particulate matter to mixing layer meteorology over the North China Plain).

We deeply thank the reviewers for giving constructive comments and suggestions that are very helpful to improve our manuscript. The comments raised by the reviewers mostly focus on five aspects: 1) observation data profile description; 2) calculation method of occurrence frequency and MLH; 3) a case study of the typical $PM_{2.5}$-O_3 co-polluted episode; 4) influence of WS and WD; 5) limitation of this work. We have answered these comments point by point and listed in the following pages.

On behalf of all the co-authors, I would like to thank you and referees for all the invaluable comments. Please feel free to contact me if you need any further information.

Yours Sincerely,

Jian Gao

Professor

Chinese Research Academy of Environmental Sciences, Beijing 100012, China

E-mail address: gaojian@craes.org.cn

Phone: 18911819868

1. Observation data profile description

Reviewer #2: Lack of data profile description. For example, how many observatories are there, and what observation elements do each station have? The author should at least add a table that fully illustrates the data.

Reviewer #1: In the map of Figure 1, it is advisable to specify the exact locations of the measurements. Are they conducted within cities? What environments have been selected, and what criteria were used for their selection? Is there any measurement that could be heavily influenced by local emissions?

Line 106, the meteorological variables are measured at the same measurement site, right?

What is the temporal resolution of the meteorological measurements? Have they been averaged to obtain daily averages? It is not clear.

Answer: Our field observations were conducted based on the existing ground-level observation stations (national control station, $PM_{2.5}$ component network, etc.) in the North China Plain (NCP), which covered two megacities (BeiJ and TianJ) and 26 surrounding cities. The spatial distribution of these 28 valid sites was shown in Figure 1. Hourly concentrations of ground-level SO_2, NO_2, O_3, $PM_{2.5}$ and its chemical compositions (SO_4^{2-}, NO_3^-, NH_4^+, and OC), and meteorological variables, including air temperature, relative humidity (RH), wind speed (WS) and direction (WD), and 24-h accumulated precipitation, at the sites were obtained from the platform of National Atmospheric Particulate Chemical-Speciation-Network. This network is established to improve the understanding of the heavy pollution formation mechanism in the North China Plain (NCP) and support the decision-making of local governments and state administration. Hourly SO_2, NO_2, O_3, $PM_{2.5}$ and its chemical compositions were recorded at the $PM_{2.5}$ component network, which was selected followed the Technical Regulation for Selection of Ambient Air Quality Monitoring Station published by the Ministry of Ecology and Environment of the People's Republic of China (HJ664−2013). The monitoring sites of $PM_{2.5}$ component network were mostly set up within the cities, and can reflect the average pollution level of each city. Details for the near-ground observation stations of $PM_{2.5}$ component network were shown in Table R1. The meteorological variables were recorded in the national meteorological observation stations, and the information of each station can be obtained from the public website of China Meteorological Administration (http://data.cma.cn/data/cdcindex/cid/0b9164954813c573.html). It should be noted that the measurement sites of meteorological variables and air pollutants were not always consistent. To better analyze the meteorological conditions for O_3 and $PM_{2.5}$, only the station closed to the air quality monitoring station and representative of the city meteorological condition was selected in our work. The temporal resolution of air temperature, RH, WS and WD was 1-h. To avoid the influence of diurnal boundary layer cycles, in this article we focused on the relationships between daily mean air pollutants and meteorological factors. The daily mean meteorological factors, $PM_{2.5}$ and its major secondary components were calculated from the hourly data; daily O_3 concentration was characterized by the maximum daily 8 h average ozone (MDA8

O_3). Details for the near-ground observation species and the metrics were shown in Table R2. The above discussion has been added in our revised manuscript **(Page 6−7, line 111−143)**.

Table R1. List of observation stations and locations.

No.	Site	Abbreviation	Station	longitude (°E)	latitude (°N)
1	BeiJing	BeiJ	China National Environmental Monitoring Centre	116.41	40.04
2	Tianjin	TianJ	Zhongshan North Road Station	117.21	39.17
3	Shijiazhuang	SJZ	Northwest Shuiyuan Station	114.49	38.13
4	Langfang	LangF	Langfang Hebei University of Technology Station	116.70	39.55
5	Baoding	BaoD	Yangguang North Street Station	115.48	38.93
6	Tangshan	TangS	Xiaoshan Station	118.19	39.62
7	Handan	HanD	Guangming South Street Station	114.50	36.57
8	Hengshui	HengS	Hengshui Ecology and Environment Bureau Station	115.68	37.73
9	Xingtai	XingT	Quanbei Street Station	114.53	37.09
10	Cangzhou	CangZ	Cangzhou Technical College Station	116.82	38.28
11	Taiyuan	TaiY	Taiyuan Jinyuan Station	112.48	37.71
12	Yangquan	YangQ	Nanzhuang Road Station	113.59	37.85
13	Changzhi	ChangZ	Changzhi Ecology and Environment Bureau Station	113.11	36.20
14	Jincheng	JinC	Jincheng Ecology and Environment Bureau Station	112.86	35.49
15	Jinan	JiNan	Jinan Environmental Monitoring Station	117.06	36.66
16	Zibo	ZiB	Beijing Road station	117.91	36.84
17	Jining	JiNing	Jinyu Road Station	116.63	35.43
18	Dezhou	DeZ	Baima Lake Station	115.83	36.95
19	Liaocheng	LiaoC	Liaocheng monitoring center Station	115.98	36.50

20	Binzhou	BinZ	Binzhou Ecology and Environment Bureau Station	118.01	37.38
21	Heze	HeZ	Heze Quality Supervision Bureau Station	115.53	35.21
22	Zhengzhou	ZhengZ	Zhengzhou Forty-seven Middle School Station	113.74	34.77
23	Kaifeng	KaiF	Jinming West Street Station	114.30	34.80
24	Anyang	AnY	Anyang Ecology and Environment Bureau Station	114.40	36.09
25	Hebi	HeB	Hebi Ecology and Environment Bureau Station	114.29	35.72
26	Xinxiang	XinX	Xinxiang Ecology and Environment Bureau Station	113.92	35.30
27	Jiaozuo	JiaoZ	Fengshou Middle Road Station	113.28	35.21
28	Puyang	PuY	Jinti Road Station	115.04	35.76

Table R2. List of observation species and metrics.

Species	Unit	Temporal resolution	Metrics
Gaseous pollutants			
O_3	μg m^{-3}	1 h	Maximum daily 8 h average
SO_2	μg m^{-3}	1 h	Daily average
NO_2	μg m^{-3}	1 h	Daily average
$PM_{2.5}$ and its major components			
$PM_{2.5}$	μg m^{-3}	1 h	Daily average
SO_4^{2-}/ NO_3^-/ NH_4^+	μg m^{-3}	1 h	Daily average
OC	μg m^{-3}	1 h	Daily average
Meteorological variables			
Temperature (T)	° C	1 h	Daily average
Relative Humidity (RH)	%	1 h	Daily average
Wind speed (WS)	m s^{-1}	1 h	Daily average
Wind direction (WD)	°	1 h	Daily average
24-h precipitation	mm	24 h	24-h accumulated

2. Calculation method of the occurrence frequency

Reviewer #2: Figure 2 is confusing. My understanding is that the proportion of different values occurring at a certain time should sum to 100%. But the sum expressed in the figure must be more than 100%.

Reviewer #1: The % ratio of occurrence shown in Figure 2 should be mentioned in the methodology. How has it been calculated?

Answer: We have added the calculation method of the occurrence frequency (%) mentioned in Figure 2 in the methodology **(Page 7, line 144−150)**. To better demonstrate the overall change characteristics of regional air pollution and meteorological conditions during the observation period, the occurrence frequency (%), which means the proportion of the number of cities at each air pollutant or methodology level, was calculated based on the following equation:

$$\text{Occurrence frequency}_{X}^{level} = \frac{N_{X}^{level}}{\text{Total } N_X} \times 100\% \quad (1)$$

where X means the air pollutant or methodology factors, N_{X}^{level} represents the number of cities at each X level, $\text{Total } N_X$ represents the total number of cities. For example, as for the MLH condition, the MLHs were classified into 8 levels, and this ratio indicates the proportion of the number of cities at each MLH level to the total number of cites. As can be seen in Figure 2, on June 5, 2021, the proportion of the number of cities at MLH>2100 m was around 85 %, and significantly higher than other MLH conditions; on June 10, 2021, the MLH in all cities were lower than 1200 m, with the ratio at MLH<1200 as 100%.

3. Calculation method of MLH

Reviewer #2: In view of the importance of MLH, the authors have not confirmed the calculation results. The authors use a very simple method to calculate the height of the mixed layer. It is suggested that the author make use of the meteorological profile or ERA5 reanalysis data to verify the reliability of the results.

Generally, when the boundary layer rises, the wind speed will increase, especially when the boundary layer exceeds 1500 m, but this phenomenon is not shown in this study. In addition, in general, when precipitation occurs, strong convection occurs, and the height of the mixing layer will suddenly rise, which is different from the author's study. Therefore, it is highly recommended that the authors validate the results of mixing layer height.

Reviewer #1: Point 2.2. The methodology for calculating the MLH seems somewhat simplistic. While estimating MLH can be complex, it would be advisable to compare the results with sounding data (already shown) or reanalysis data to determine their coherence with the calculated values.

Answer: Even though the method for calculating MLH in this work seems simple, this methodology reflects the basic physical nature of the pollution mixing layer height. In recent years, many works have progressed in the atmospheric boundary layer characteristics, and analyzed the impacts of these parameter on air pollution. Planetary boundary layer (PBL), as one of the critical parameters to air quality modeling, has been well explored. However, PBL usually refers to the large-scale Ekman dynamic boundary layer (Haugen et al., 1971; Wang et al., 2014; Zhang et al., 2005). The way with which boundary layer describes the influences of air pollution is

easily duplicated and confused (Niu et al., 2017). It is unreasonable to some extent, if the characteristic of the air pollution related to near-surface boundary layer is evaluated by using the concept of PBL. For air pollution measurement, one of selected functionalities of parameterization scheme for pollution mixing layer is to judge whether an air mass over a specific locality satisfies the "static and stable" attribute or not. Therefore, in this work, to express the basic physics for diagnosing meteorological conditions, we used the concept of pollution mixing layer height (MLH) proposed by Wang et al. (2017), which was based on the classical synoptic theory according to the level of convective condensation layer, and the details of this method can be seen in previous work (Wang and Yang, 2000; Wang et al., 2017).

To be specific, we defined the height close to the cloud base as the height of super-saturation layer (H_SSL), and the isoentropic atmospheric process meets the level of convective condensation layer (LCL) in the super-saturation state, i.e., it is very close to the H_SSL. Iterative algorithm is used to work out the H_SSL (Wang and Yang, 2000):

$$\mathrm{H\_SSL} \approx \mathrm{LCL} = 6.11 \times 10^2 \times \left(\frac{0.622 + 0.622 \frac{e_s}{p - e_s}}{0.622 \frac{e_s}{p - e_s}} \right) \quad (2)$$

$$e_s = 6.22 \times \exp \frac{17.13(T - 273.16)}{T - 38} \quad (3)$$

where e_s represents saturated water vapor pressure, T is temperature (K). Eq. (2) can be used to calculate the H_SSL which is favorable for pollutant mixing and represented by (P). Below this height, the atmosphere gets supersaturated, causing the pollution mixing and wetting process in the low altitude to continue, so this height is also called the height of pollution mixing layer (MLH). Thus, MLH can be derived in the following expression:

$$\mathrm{MLH} \approx \mathrm{H\_SSL} \approx \mathrm{LCL} = 6.11 \times 10^2 \times \left(\frac{0.622 + 0.622 \frac{e_s}{p - e_s}}{0.622 \frac{e_s}{p - e_s}} \right) \quad (4)$$

According to the relationship between air pressure and height, the units of MLH can be converted to the height expression in meters:

$$\int_{p_0}^{p_z} dp = -\int_0^z \rho_0 g dz, \quad (5)$$

where z is the height, ρ_0 is the density of gas, p_z and p_0 represent the air pressure in the height of z and 0, respectively.

Several works have verified the reliability of the results based on this method. With this method, Wang et al. (2017) well characterized the features of mixing layer height in highly-sensitive areas of pollution in China (1−31 December 2015 for Beijing and the same period of 1−31 December 2015 for Guangzhou), and demonstrated the schematic diagram of 3-D model for low-level super-saturation layer and pollution mixing layer in the pollution hotspots in China, such as North China Plain (NCP), Yangtze River Delta (YRD), Pearl River Delta (PRD) and Si-Chuan Basin (SCB). Wang et al. (2022) also used this method to explore the $PM_{2.5}$ and O_3 superposition-composite pollution event during spring 2020 in Beijing, China,

and the hourly evolution of MLH, O_3, and $PM_{2.5}$ during the observation period were analyzed. The results can well depict the MLH diurnal cycle, which rises at daytime and decreases at night. In addition, Niu et al. (2017) has applied this method in Beijing, and the results showed that the pollution mixing layer can well present the change characteristics of haze pollution process. In this work, we further clarified the concept of MLH, and applied this method to investigate the impacts of MLH upon the change characteristics of ozone and fine particulate matter. The above discussion has been added in our revised manuscript **(Page 7−8, line 152−190)**.

As we known, there are differences between MLH and PBLH (Height of planetary Boundary layer). These phenomena ("when the boundary layer rises, the wind speed will increase, especially when the boundary layer exceeds 1500 m", "when precipitation occurs, strong convection occurs, and the height of the mixing layer will suddenly rise") were generally summarized based on PBLH in individual cases. Besides, these phenomena can not fit each case, and there are still exceptions. We have added the change characteristics of wind speed (WS) along with the increase of MLH (Figure R1). Actually, we can see apparent increase of WS when MLH in the range of 0−300 m which was probably due to precipitation events. The increase of WS when MLH exceeds 1500 have also been observed, but the increment was not so obvious. Previous works by Liu and Liang (2010) and Li et al. (2020) have found that the severe convective weather generally decreases PBLH, and the precipitation was highly negatively correlated with PBLH, which was consistent with the results found in our work. The rainfall events may produce clouds, then reduce surface solar and thermal heating, thus suppressing the PBLH.

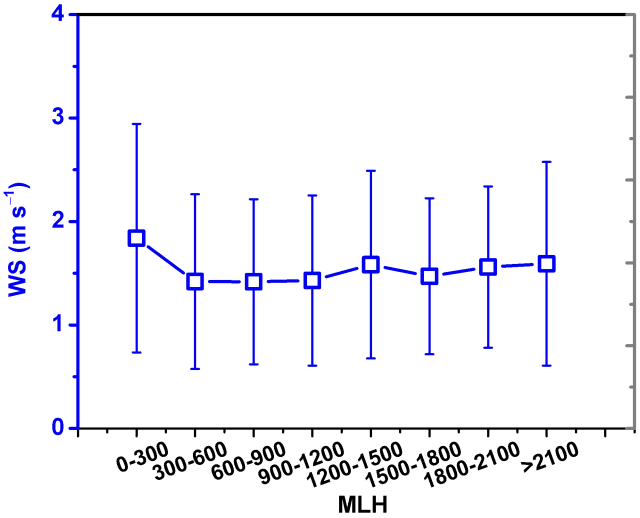

Figure R1. The change characteristics of WS under different MLH conditions.

4. A case study of the typical $PM_{2.5}$-O_3 co-polluted episode

Reviewer #2: The authors need to find a case to fully present the relationship between the mixing layer and pollutants, and use the hourly concentration to illustrate the response of PM, its components and ozone to the mixing layer.

Reviewer #1: Concentrations of daily averages are also analyzed, but in this kind of

episodes, the relevance of hourly concentrations can be crucial. This should also be made clear somewhere, although the analysis of the episodes is only carried out to highlight certain results.

Answer: We find a typical $PM_{2.5}$-O_3 coordinated event (Episode II: June 18–29, 2021) during the observation period to comprehensively present the relationship between the mixing layer meteorology and air pollutants. Figure R2 and R3 showed the temporal-spatial distribution of air pollutants and meteorological factors during June 18−29, 2021. On June 18−20, MLH gradually increased from 600−1200 m to 1500−3000 m in the southern and eastern part of the NCP, $PM_{2.5}$ and MDA8 O_3 concentrations concurrently increased and showed similar spatial distributions. The wind speed dropped significantly on 20 June, and the value was lower than 1 m s^{-1} in most cities. On 21−23 June, MLH started to decrease from 1500−3000 m to 1200−1800 m, $PM_{2.5}$ and MDA8 O_3 concentrations further increased, and the areas of high $PM_{2.5}$ concentrations coincided well with those of MDA8 O_3 concentrations. During 24−25 June, MLH continued to decrease, with some values even lower than 300 m. The MLH for the areas with high MDA8 O_3 was in the range of 900−1500 m. Interestingly, the synchronized spatial change characteristics of $PM_{2.5}$ and MDA8 O_3 were consistent when MLH in the range of 900−1200 m, while inconsistent when MLH lower than 600 m. Significant rise of $PM_{2.5}$ concentration was observed in some cities with MLH lower than 300 m. It's noted that the dominant chemical composition of $PM_{2.5}$ in these areas was NO_3^-. On 28 June, the rise in MLH was observed in the central and the southern part in the NCP, and a surge of MDA8 O_3 and $PM_{2.5}$ concentrations both occurred, with 160−220 μg m^{-3} and 40−50 μg m^{-3} respectively. In general, most cities were dominated by weak winds from the east and southeast, which favored the formation of secondary pollutants from the gaseous precursors transported from the southeast part and promoted the accumulation of air pollutants.

To better understand this $PM_{2.5}$-O_3 co-polluted event, here we classified the observations during this typical event into four categories: O_3 polluted days (O_3PD; MDA8 O_3 concentration > 160 μg m^{-3} and $PM_{2.5}$ < 35 μg m^{-3}), $PM_{2.5}$ polluted days ($PM_{2.5}$PD; MDA8 O_3 concentration < 160 μg m^{-3} and $PM_{2.5}$ > 35 μg m^{-3}), O_3–$PM_{2.5}$ co-polluted days (O_3–$PM_{2.5}$CPD; MDA8 O_3 concentration > 160 μg m^{-3} and $PM_{2.5}$ > 35 μg m^{-3}), and non-polluted days (NPD; MDA8 O_3 < 80 μg m^{-3} and $PM_{2.5}$ < 35 μg m^{-3}). Figure R4 showed the meteorological and chemical characteristic of O_3–$PM_{2.5}$ CPD, O_3 PD, $PM_{2.5}$ PD, and NPD. The results indicated that the values of MLH on O_3–$PM_{2.5}$CPD were between those on O_3PD and $PM_{2.5}$PD at around 900 m. On O_3–$PM_{2.5}$CPD, the oxidation ratio of sulfate (SOR, the molar ratio of sulfate to the sum of sulfate and SO_2) and oxidation ratio of nitrate (NOR, the molar ratio of nitrate to the sum of nitrate and NO_2) were the highest, with the values of 0.44 and 0.33, respectively, which indicated the strong secondary formation of SO_4^{2-} and NO_3^- promoted by high O_3 concentration. The $PM_{2.5}$PD occurred when MLH lower than 650 m, and the percentage of NO_3^- was the highest on $PM_{2.5}$PD. The rise of $PM_{2.5}$ in some cities under low MLH conditions may be attributed to three mechanisms. The first one is the accumulation effect due to unfavorable diffusion condition when MLH

decreased. Second, these cities got little rain, and the effect of wet deposition was weak. In addition, the corresponding low T and high RH can stimulate the formation of NO_3^- from gaseous state (HNO_3). On O_3PD, the MLH was at around 1300 m, and the NOR turned to decrease, demonstrating a more significant role of partitioning process between gas and aerosol than the atmospheric oxidation process under this stage. On NPD, the MLH was the highest, with the value of about 2400 m, and the $PM_{2.5}$ chemical composition was obviously dominated by OM.

To explore the relevance of hourly O_3, $PM_{2.5}$, its components and MLH, we have taken PuY and HeZ as examples. Figure R5 plotted the day-to-day variations along with the diurnal variations of O_3, $PM_{2.5}$, its components and MLH in PuY and HeZ during Episode II (June 18−29, 2021). The results showed that there were large diurnal as well as day-to-day variability in the O_3 and $PM_{2.5}$ levels. The diurnal variations of MLH were clearly visible (Figure R6), with the rise in MLH during the daytime and the decrease in MLH at night. The concentration of $PM_{2.5}$ increased with the decrease of MLH at night, but the concentration of O_3 increased with the rise of MLH at daytime. Interestingly, we observed noontime soar of SO_4^{2-} and OC concentrations in PuY, and the values of SOR kept stable or even increased at noon. Besides, it's noted that daily O_3 and $PM_{2.5}$ both gradually accumulated with the increase of MLH during June 18−21 and 26−28, which can be attributed to the O_3 and $PM_{2.5}$ superposition composite effects. The decrease in $PM_{2.5}$ at daytime with the rise of MLH can be partly offset by an increment in secondary pollutants formation derived from O_3 growth. Then with the decrease of MLH at night, the concentration of the original existing $PM_{2.5}$ increased due to unfavorable diffusion. In general, the conclusions in this work was only suitable to the day-to-day relationship between air pollutants and MLH. The hourly relationships were more complicated and need more further analysis. According to these valuable comments, we will further explore the hourly relationship in the NCP in our follow-up studies. The above discussion has been added in our revised manuscript **(Page 19−24, line 393−476)**.

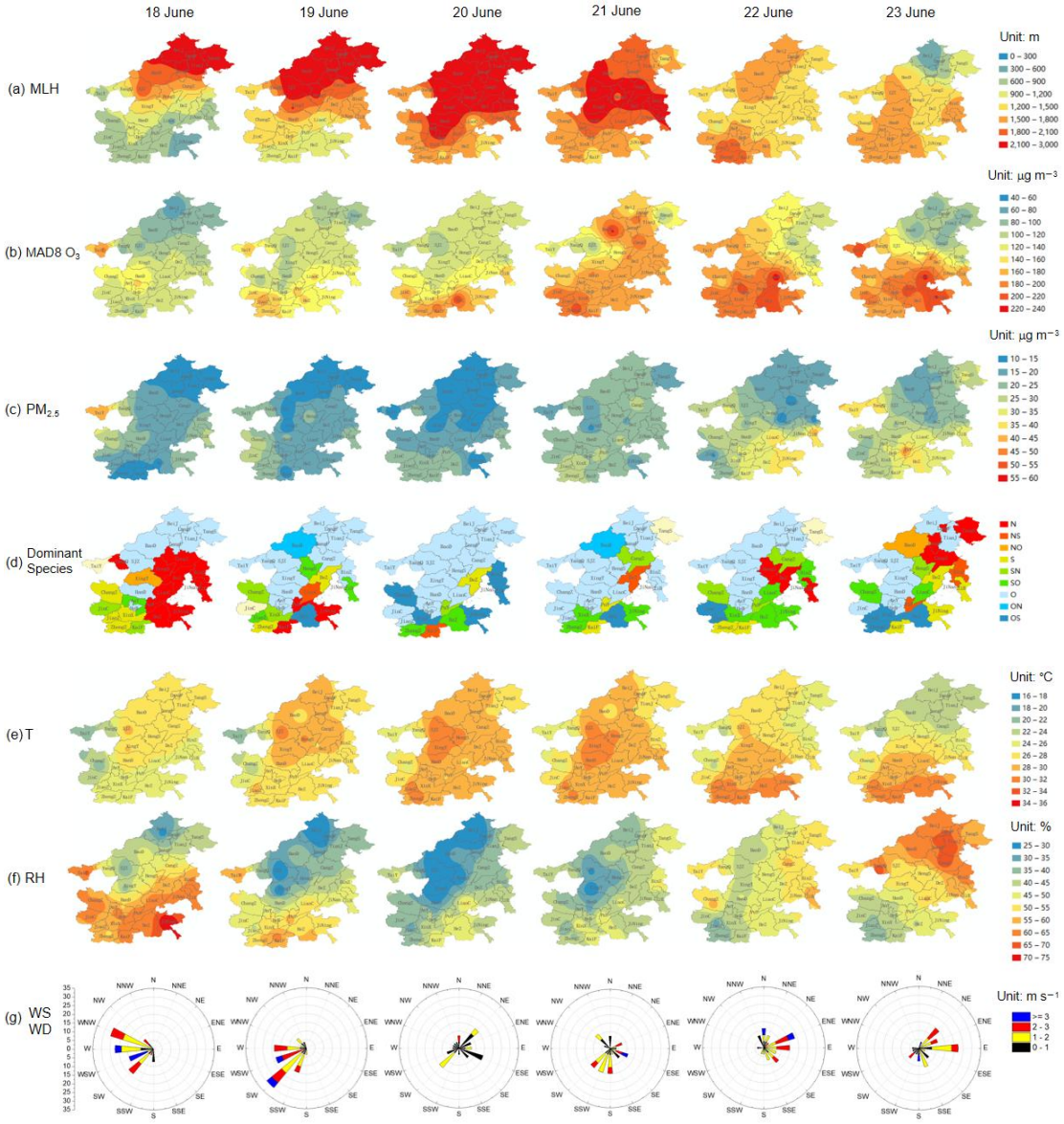

Figure R2. The spatial distribution of (a) MLH, (b) MDA8 O_3, (c) $PM_{2.5}$, (d) the dominant $PM_{2.5}$ chemical component (N: NO_3^- dominant, NS: NO_3^- and SO_4^{2-} dominant, NO: NO_3^- and OM dominant, S: SO_4^{2-} dominant, SN: SO_4^{2-} and NO_3^- dominant, SO: SO_4^{2-} and OM dominant, O: OM dominant, ON: OM and NO_3^- dominant, OS: OM and SO_4^{2-} dominant), (e) T, and (f) RH, (g) the overall change characteristics of WS and WD in the NCP from June 18 to 23, 2021.

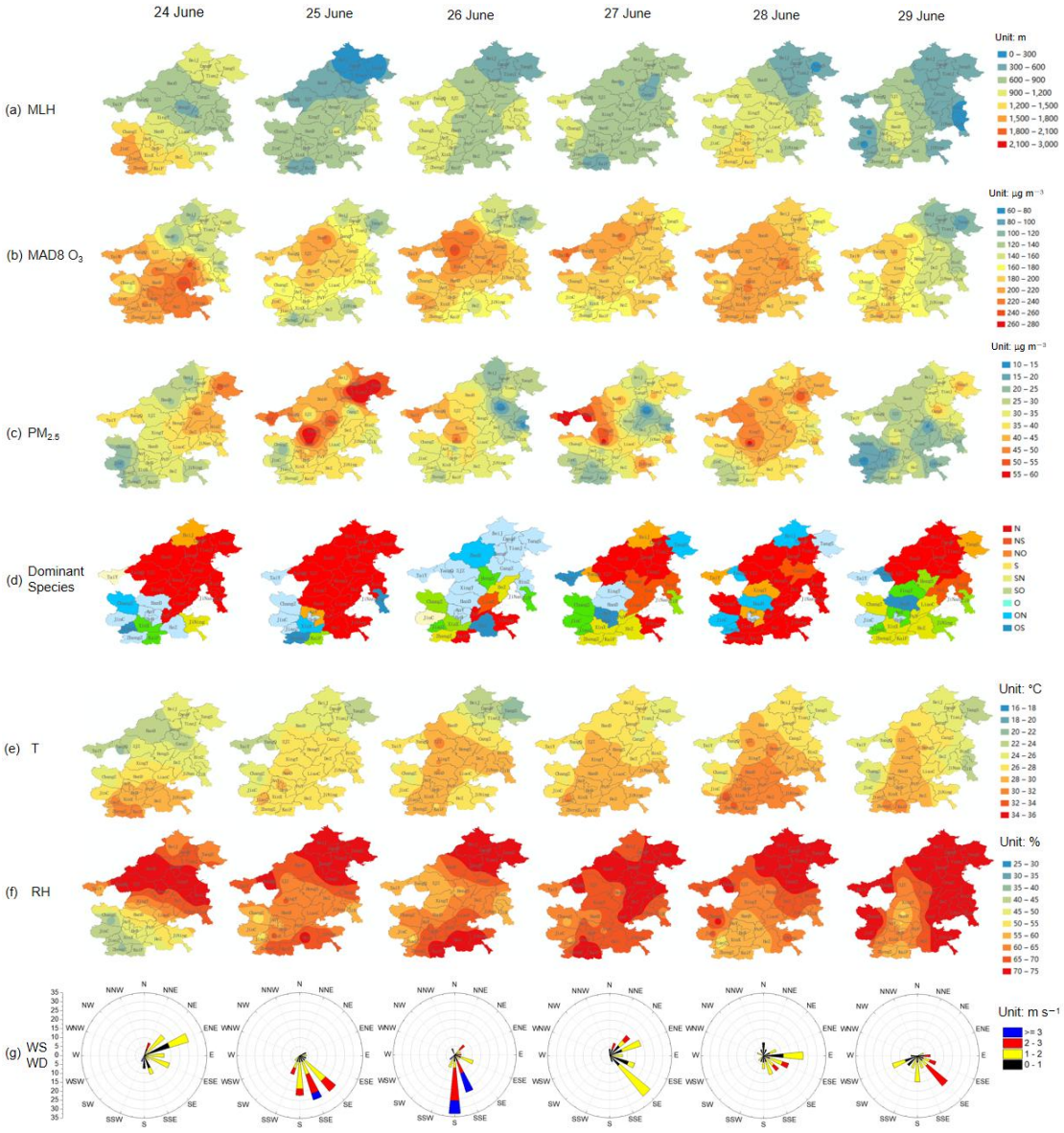

Figure R3. The spatial distribution of (a) MLH, (b) MDA8 O_3, (c) $PM_{2.5}$, (d) the dominant $PM_{2.5}$ chemical component (N: NO_3^- dominant, NS: NO_3^- and SO_4^{2-} dominant, NO: NO_3^- and OM dominant, S: SO_4^{2-} dominant, SN: SO_4^{2-} and NO_3^- dominant, SO: SO_4^{2-} and OM dominant, O: OM dominant, ON: OM and NO_3^- dominant, OS: OM and SO_4^{2-} dominant), (e) T, and (f) RH, (g) the overall change characteristics of WS and WD in the NCP from June 24 to 29, 2021.

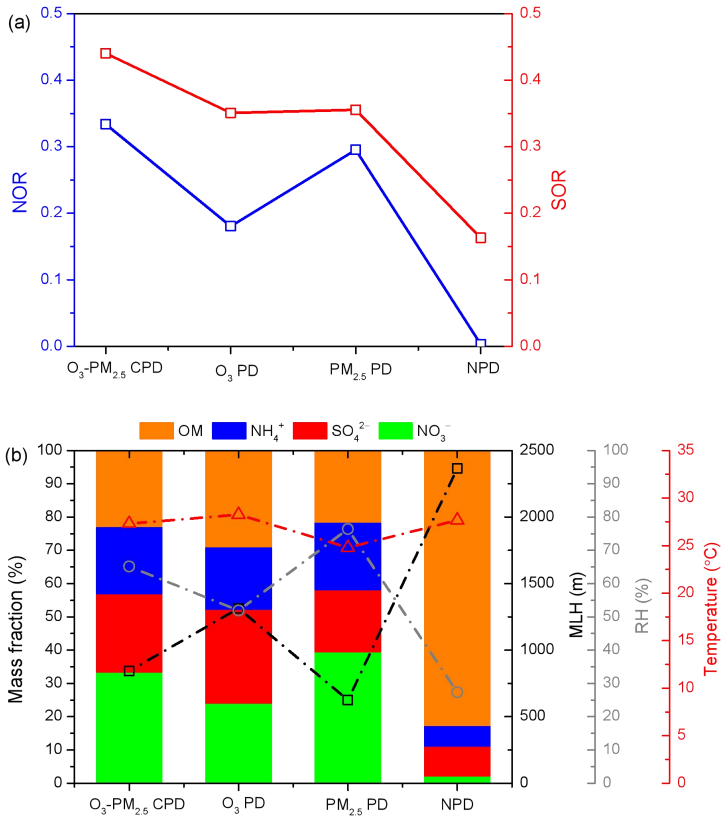

Figure R4. The distribution characteristics of (a) NOR and SOR, and (b) the mass fractions of major $PM_{2.5}$ components, MLH, RH, and T under O_3–$PM_{2.5}$ CPD, O_3 PD, $PM_{2.5}$ PD, and NPD conditions from June 24 to 29, 2021.

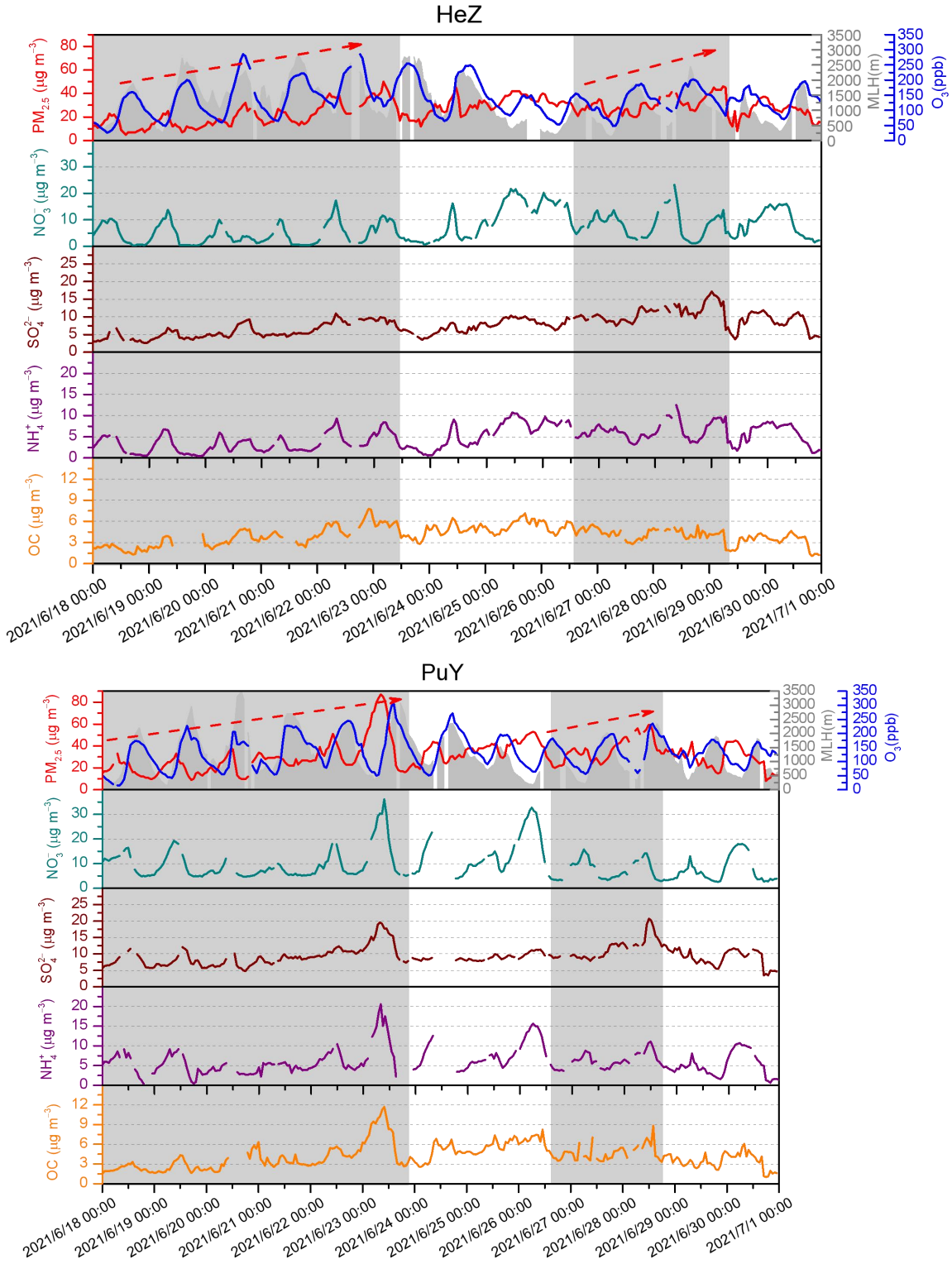

Figure R5. The hourly evolution of O_3, $PM_{2.5}$, its components and MLH in HeZ and PuY during June 18–29, 2021.

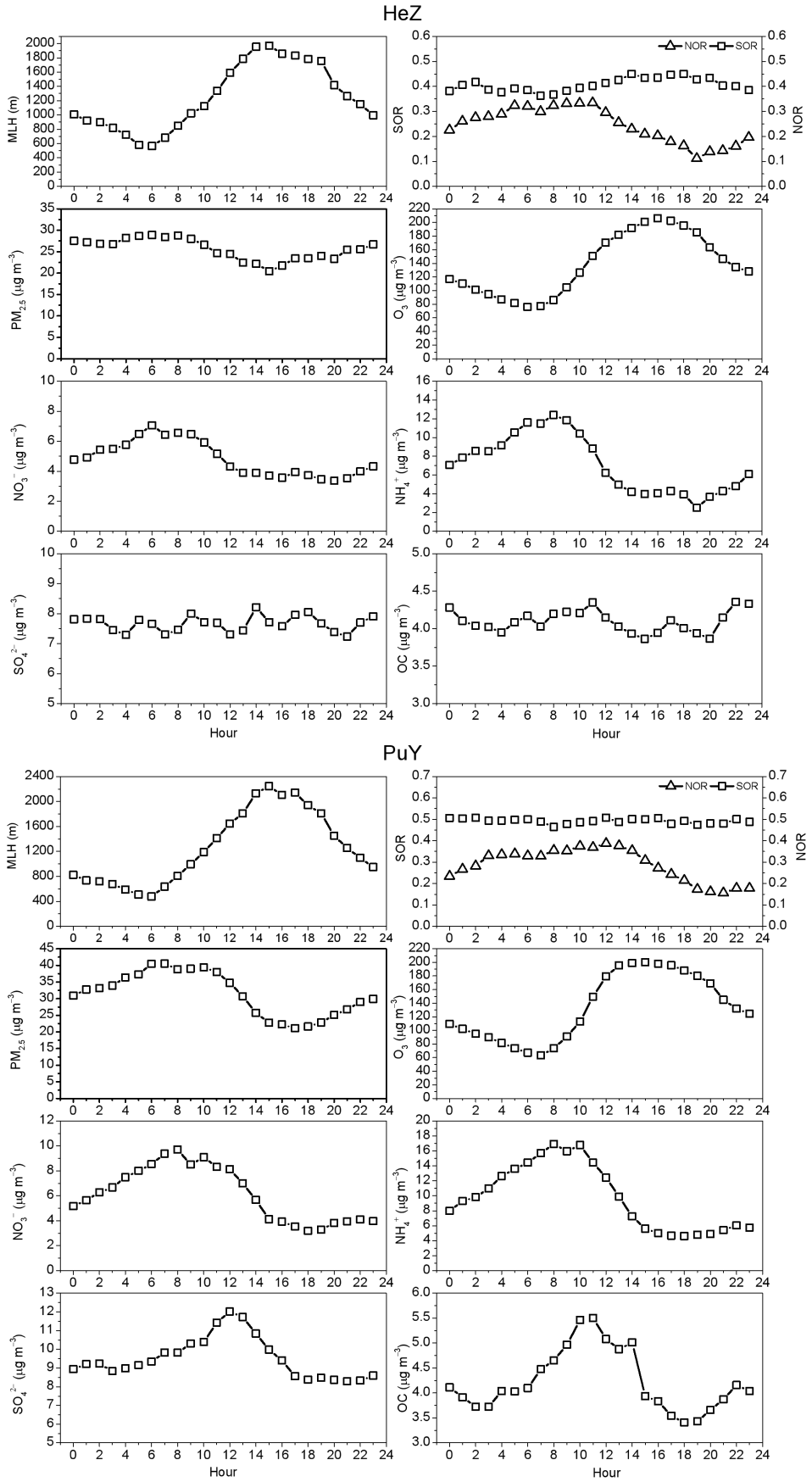

Figure R6. The diurnal variation of MLH, SOR, NOR, O_3, $PM_{2.5}$, and its components in HeZ and PuY during June 18−29, 2021.

5. The influence of WS (Wind Speed) and Wind Direction (WD)

Reviewer #1: The WS (Wind Speed) is barely mentioned, and I miss the Wind Direction. Although the authors discard advection, how can authors be certain that it is not always due to the same emission source or the same synoptic pattern?

Answer: To reveal the impact of wind on the variation trends of air pollution, we presented the results of wind speed (WS) and wind direction (WD) in our revised manuscript (Figure R7– R11). As shown in Figure R7, during the whole campaign, the NCP was dominated by winds from northeast and south (45–225°). Because more than 75 % WD were in the rang of 45–225°, the WD was classified into 4 categories: 45–90, 90–135, 135–180, and 180–225°. To further investigate the impact of wind on MDA8 O_3 and $PM_{2.5}$ concentrations, we also demonstrated the statistics on the concentration distributions of MDA8 O_3, $PM_{2.5}$ and its dominant components with the increase of MLH under different WS and WD conditions in Figure R9–R11. In general, WS could affect the diffusion of air pollutants. During the observation period, WS was mostly less than 3 m s^{-1}, and the concentrations of air pollutants were comparatively higher at low wind speeds. As shown in Figure R8, at low MLH conditions (MLH<300 m), a northeasterly wind prevailed near the ground, and the WS was generally higher than other conditions. The concentration of MDA8 O_3 was low during this period. With the increase of MLH, the WD gradually changed from northeast (MLH=300–600 m) to southeast (MLH=600–900 m) and south (MLH=900–1200 m). The North China Plain (NCP) is surrounded to the west by the Taihang Mountains, to the north by the Yan Mountains, and to the east by the Bohai Sea (Figure 1). The southerly wind can transport the gaseous pollutant or O_3 from the southern part of the plain area to the northern part, and the Taihang mountains may block pollutant transport, leading to the accumulation of pollutants along the foot of the Taihang Mountains. It's noted that the concentration of MDA8 O_3 was higher when the plain dominated by southerlies (180–225°) (Figure R9). When MLH higher than 2100 m, NCP was governed by northwest winds, which preferred the outward transport and diffusion of pollution, leading to the decrease of MDA8 O_3. Comparing with O_3, the impact of WD along with the increase of MLH seems different for $PM_{2.5}$ and its dominant components. When MLH in the range of 600–1200 m, the NCP was dominated by southeast or south winds. However, when southeast or south wind prevailed, the corresponding $PM_{2.5}$ and its dominant components concentrations were comparable or even lower than other WD situations (Figure R10–R11). This indicated that regional transport was not the dominant factor leading to the elevation of $PM_{2.5}$ and its aerosol species along with the evolution of mixing layer (MLH < 1200 m). The above discussion has been added in our revised manuscript **(Page 12−13, line 271−283; Page 18, line 377−383;)**.

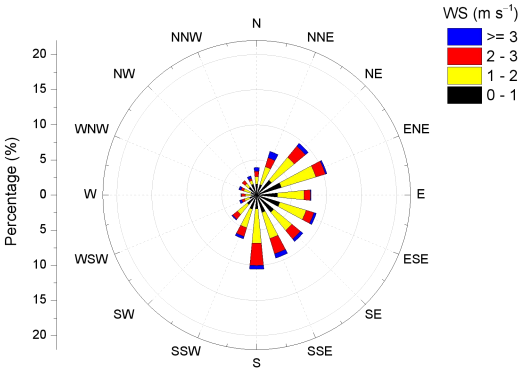

Figure R7 The overall WS and WD condition during the observation campaign. S: south; N: north; E: east; W: west.

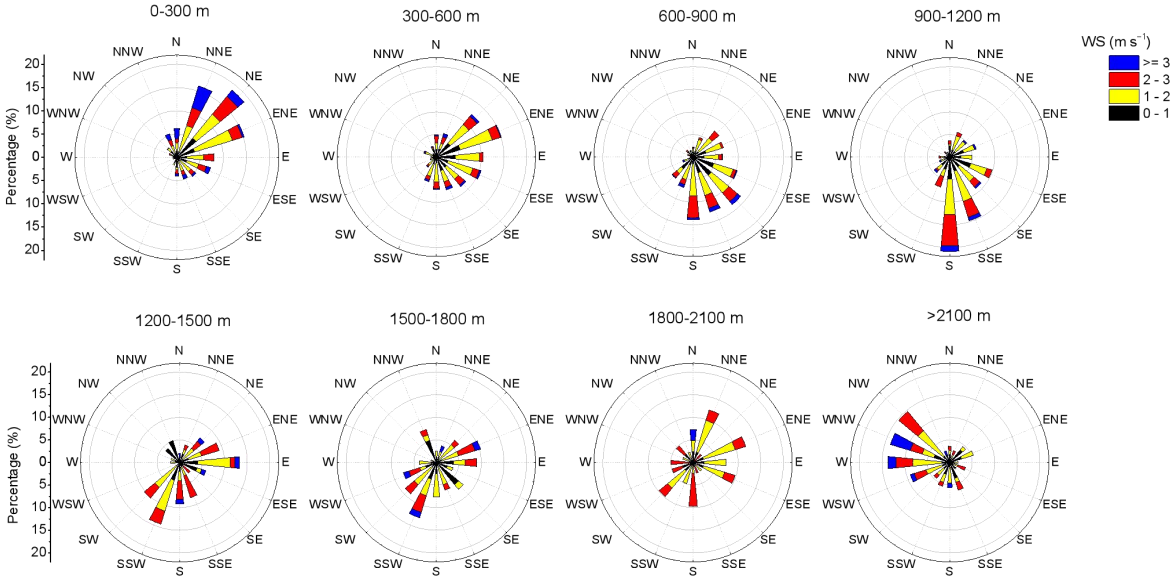

Figure R8 The change characteristics of WS and WD under different MLH levels. S: south; N: north; E: east; W: west.

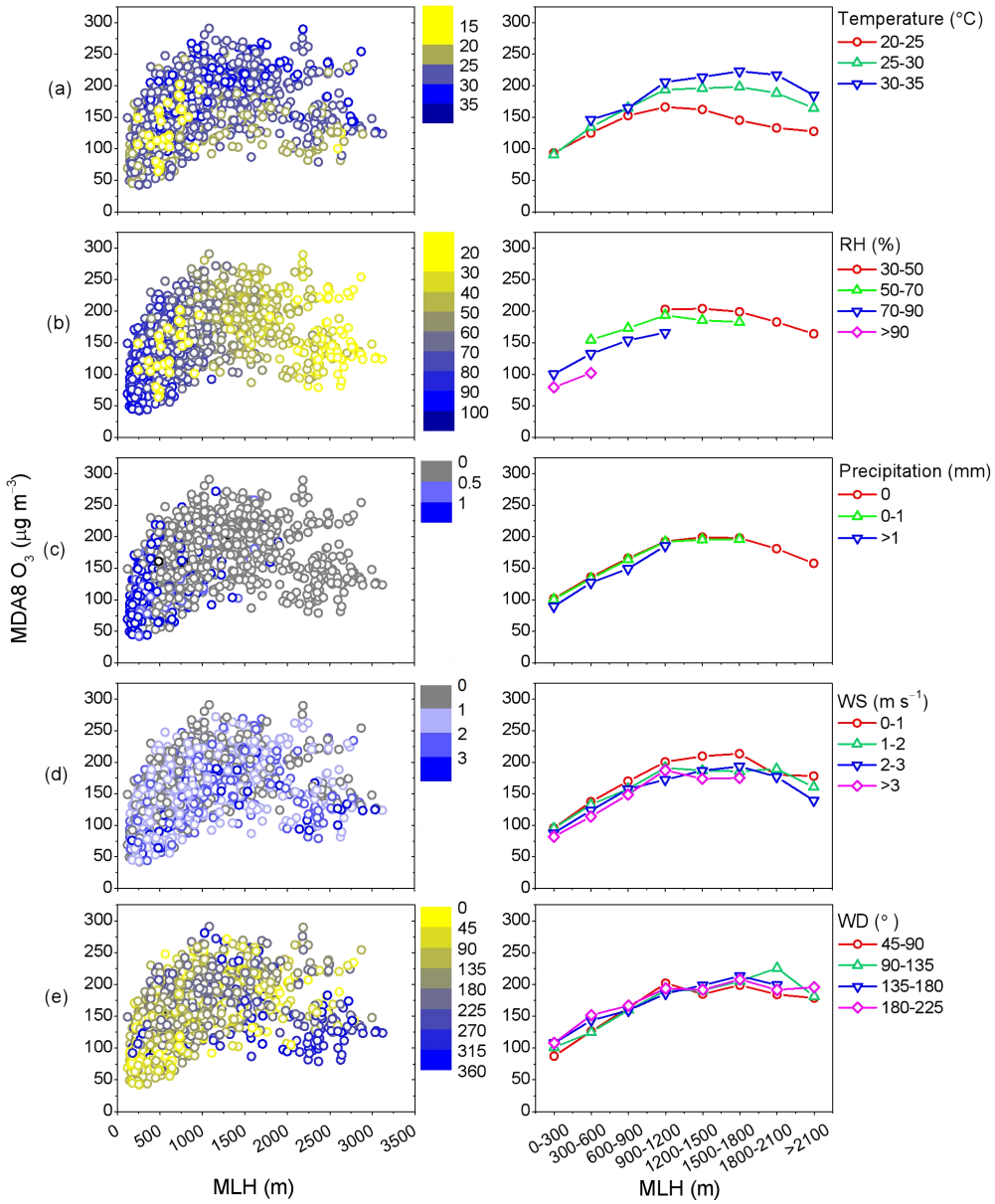

Figure R9. The distribution characteristics of the MDA8 O_3 concentrations with the evolution of MLH under different (a) temperature, (b) RH, (c) precipitation, (d) WS, and (e) WD conditions.

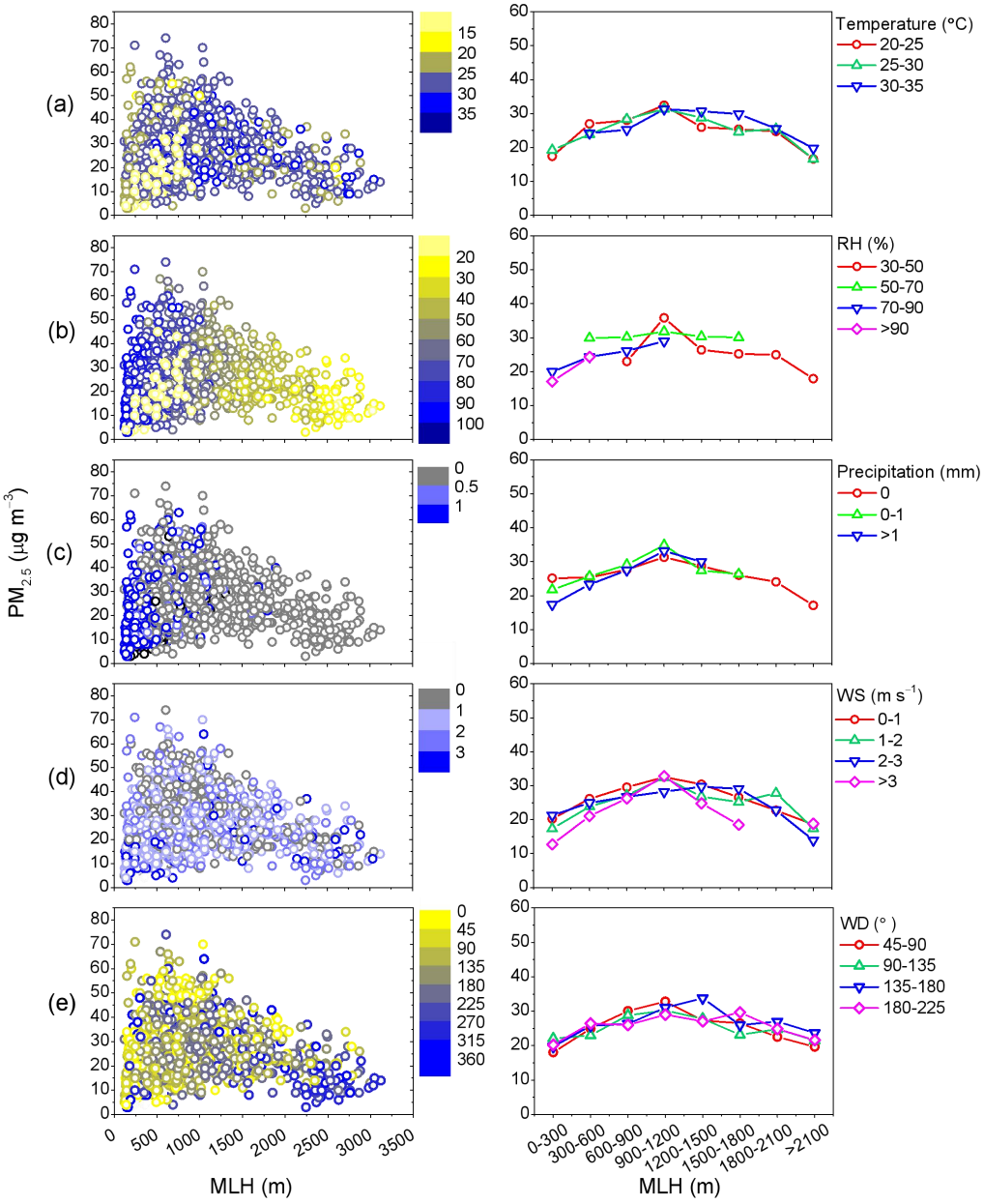

Figure R10. The distribution characteristics of the $PM_{2.5}$ concentrations with the evolution of MLH under different (a) temperature, (b) RH, (c) precipitation, (d) WS, and (e) WD conditions.

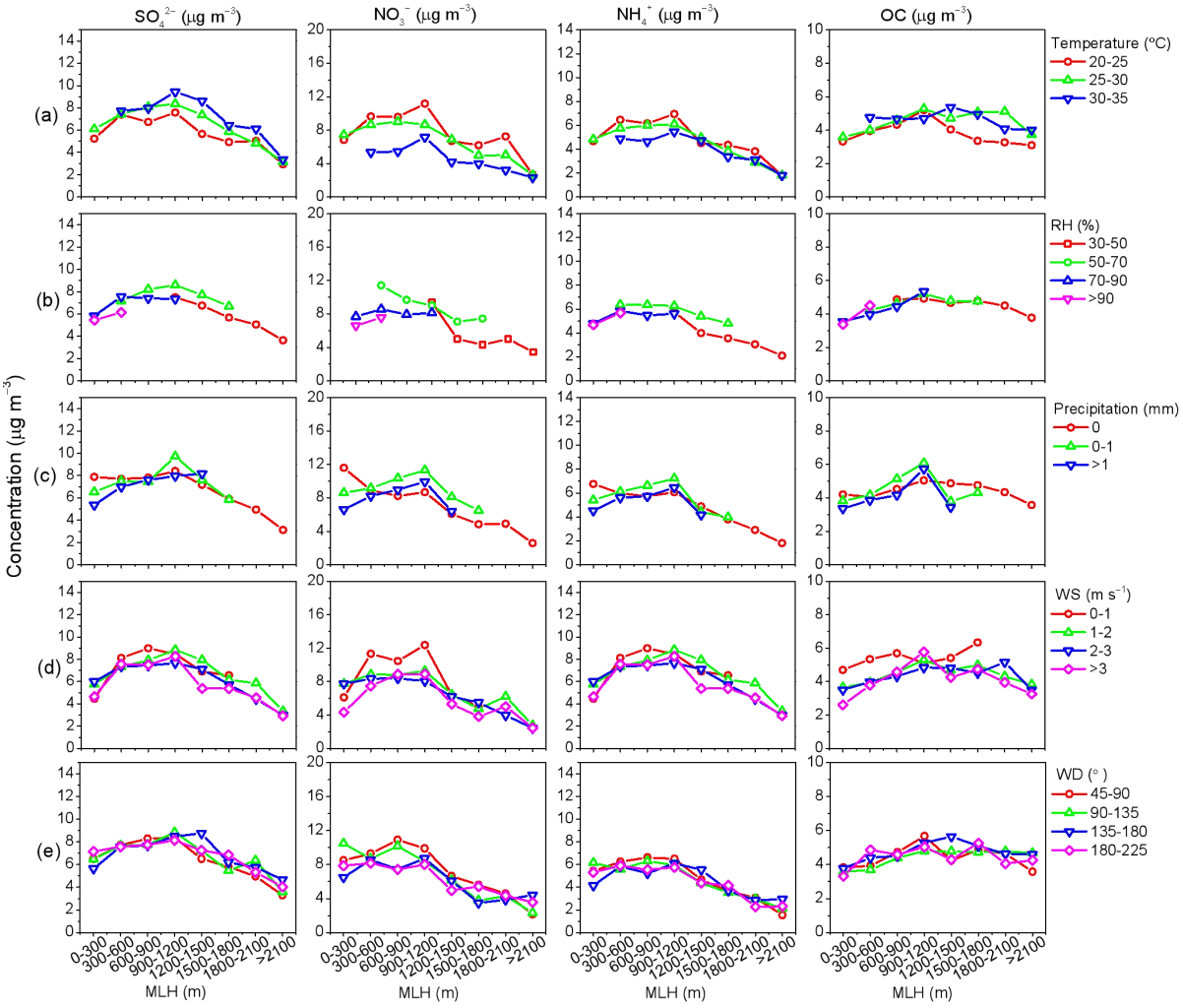

Figure R11. The distribution characteristics of NO_3^-, SO_4^{2-}, NH_4^+, and OC concentrations with the evolution of MLH under different (a) temperature, (b) RH, (c) precipitation, (d) WS, and (e) WD conditions.

6. Limitation of this study

Reviewer #1: There is a noticeable absence of indication regarding potential limitations and uncertainties in this study.

The analyzed results are limited to only two summer months, which may not be easily extrapolated to other summers. It is essential to address why the three mentioned episodes are relevant and whether the selected two months are representative of typical patterns observed throughout the years. Were there any meteorological anomalies during this period? These aspects should clear throughout the entire manuscript to provide a more comprehensive understanding of the study's scope and implications.

Answer: According to the hourly concentrations of $PM_{2.5}$ and MDA8 O_3 in China over the years of 2013–2020, the observed numbers of O_3 polluted days (MDA8 O_3 concentration $> 160\ \mu g\ m^{-3}$ and $PM_{2.5} < 75\ \mu g\ m^{-3}$), $PM_{2.5}$ polluted days (MDA8

O_3 concentration < 160 μg m^{-3} and $PM_{2.5}$ > 75 μg m^{-3}), and O_3–$PM_{2.5}$ co-polluted days (MDA8 O_3 concentration > 160 μg m^{-3} and $PM_{2.5}$ > 75 μg m^{-3}) were highest in the North China Plain (NCP). Besides, O_3–$PM_{2.5}$ co-polluted days and O_3 polluted days were generally occurred in June and July (Dai et al., 2023). Therefore, we considered the months of June and July can well represent the typical characteristics of O_3–$PM_{2.5}$ coordinated pollution during warm seasons in the North China Plain (NCP). According to the National Ambient Air Quality Standard of China (GB3095-2012), the daily $PM_{2.5}$ averages in "2+26" cities can meet the Level II national ambient air quality standard (75 μg m^{-3}), while exceeding the level I standard of 35 μg m^{-3}. Here, we defined a O_3–$PM_{2.5}$ co-polluted episode as a set of continuous days (longer than 4 days) with MDA8 O_3 and daily mean $PM_{2.5}$ in more than 10 % NCP cities exceeding 160 μg m^{-3} and 35 μg m^{-3}, respectively. According to this criterion, three typical O_3–$PM_{2.5}$ co-polluted episodes were selected: June 4–14 (Episode I), June 18–29 (Episode II), and July 2–11 (Episode III), 2021. These three episodes have been marked in Figure 2 in our revised manuscript. Comparing with the same observation period in 2020, the temperature was slightly higher and more precipitation evens happened during the summertime in 2021 (National Bulletin of Atmospheric Environment, 2021; http://www.nmc.cn/publish/environment/National-Bulletin-atmospheric-environment.htm). This work can provide an overall diagnosis of the response of ozone and fine particulate matter to mixing layer meteorology during summertime, especially in warm and humid seasons, in the NCP.

This work can gain new insights into the underlying causes of the summertime O_3–$PM_{2.5}$ coordinated pollution through exploring the response of ozone and fine particulate matter to mixing layer meteorology over the North China Plain from June 1 to July 31, 2021. However, there remained some limitations and uncertainties. First, the present study was only confined to summertime conditions (including two summer months) in the NCP, and the conclusions was likely to be different in other seasons and regions. Thus, more extended observations in time and space should be needed in the future. Second, to avoid the influence of diurnal boundary layer cycles, in this article we focused on the relationships between daily mean air pollutants and meteorological factors. We have also taken PuY and HeZ as examples to explore the relevance of hourly O_3, $PM_{2.5}$, its components and MLH. The results showed large diurnal as well as day-to-day variability in the O_3 and $PM_{2.5}$ levels. The decrease in $PM_{2.5}$ at daytime with the rise of MLH can be partly offset by an increment in secondary pollutants formation derived from O_3 growth. In general, the conclusions in this work was only suitable to the day-to-day relationship between air pollutants and MLH. The hourly relationships were much more complicated and need more further analysis. Lastly, a weakness of this study is that we did not quantify the sensitivity of O_3 and $PM_{2.5}$ to different meteorological factors and chemical processes, thus a more detailed consideration with the aid of modeling would be needed in the future. Such an exploration requires efforts going beyond the current project, and it is therefore not pursued. The above discussion has been added in our revised manuscript. **(Page 21, line 449−451; page 26, line 521−525; page 28, line 558−564)**

References

Dai, H., Liao, H., Li, K., Yue, X., Yang, Y., Zhu, J., Jin, J., Li, B., and Jiang, X.: Composited analyses of the chemical and physical characteristics of co-polluted days by ozone and $PM_{2.5}$ over 2013–2020 in the Beijing–Tianjin–Hebei region, Atmos. Chem. Phys., 23, 23-39, 10.5194/acp-23-23-2023, 2023.

Haugen, D. A., Kaimal, J. C., Bradley, E. F.: An experimental study of Reynolds stress and heat flux in the atmospheric surface layer, Q. J. Roy. Meteor. Soc., 97, 168-180, 1971.

Li, Y., Zhang, H., Zhang, Q., Zhang, A., Yang, J., Zhang, C.: Response characteristics of atmospheric boundary layer height to summer monsoon activity and monsoon precipitation of monsoon swing region in the eastern part of northwest China, Arid Land Geography, 2020, 43,1169-1178

Liu, S. and Liang, X.: Observed diurnal cycle climatology of planetary boundary layer height, J. Clim., 23, 5790-5809, 2010.

Niu, T., Wang, J., Yang, Y., Wang, Y., and Chen, C.: A study on parameterization of the Beijing winter heavy haze events associated with height of pollution mixing layer, Adv. Meteorol., 2017, 1-11, 10.1155/2017/8971236, 2017.

Wang, J., Yang, Y.: Modern weather engineering. Meteorological Press, Beijing, 334–339, 2000.

Wang, J., Bian, L., Xiao, C.: Dynamics of ekman boundary layer over the antarctic plateau in summer, Chinese Sci. Bull., 59, 999–1005, 2014.

Wang, J., Yang, Y., Zhang, X., Liu, H., Che, H., Shen, X., and Wang, Y.: On the influence of atmospheric super-saturation layer on China's heavy haze-fog events, Atmos. Environ., 171, 261-271, 10.1016/j.atmosenv.2017.10.034, 2017.

Wang, J., Yang, Y., Jiang, X., Wang, D., Zhong, J., and Wang, Y.: Observational study of the $PM_{2.5}$ and O_3 superposition-composite pollution event during spring 2020 in Beijing associated with the water vapor conveyor belt in the northern hemisphere, Atmos. Environ., 272, 10.1016/j.atmosenv.2022.118966, 2022.

Zhang, G., Bian, L., Wang, J., Yang, Y., Yao, W., Xu, X.: The boundary layer characteristics in the heavy fog formation process over Beijing and its adjacent areas, Sci. China Earth Sci., 48, 88–101, 2005.